X-ray computed tomography of cavitating flow in a converging-diverging nozzle

Jahangir, Saad; Wagner, Evert; Mudde, Rob; Poelma, Christian

DOI
10.1115/1.861851_ch209

Publication date
2018

Document Version
Final published version

Published in
Proceedings of the 10th International Symposium on Cavitation (CAV2018)

X-ray computed tomography of cavitating flow in a converging-diverging nozzle

[1]Saad Jahangir*; [2]Evert C. Wagner; [2]Robert F. Mudde; [1]Christian Poelma

[1]*Department of Process & Energy (Faculty 3mE), Delft University of Technology, Leeghwaterstraat 21, 2628 CA Delft, The Netherlands;* [2]*Department of Chemical Engineering (Faculty of Applied Sciences), Delft University of Technology, Julianalaan 136, 2628 BL Delft, The Netherlands*

Abstract

Cavitation is a complex multiphase phenomenon, where the production of vapor bubbles leads to opaqueness of the flow. While it is nearly impossible to visualize the interior of the cavitation region with visible light, we show that with X-ray computed tomography it is possible to obtain the time-averaged void fraction distribution in an axisymmetric converging-diverging nozzle (venturi). This technique is based on the amount of energy absorbed by the material, based on its density and thickness. Time-averaged 3D reconstruction of the X-ray images is used (i) to distinguish between vapor and liquid phase, (ii) to get radial geometric features of the flow, and (iii) to quantify the local void fraction. The results show the presence of intense cavitation at the walls of the venturi, and the vapor fraction decreases downstream of the venturi with the vapor cloud.

Keywords: venturi; X-ray computed tomography; cloud cavitation

1. Introduction

Cavitation in a flow occurs when the static pressure at a given location in the flow drops below the vapor pressure of the liquid. If a cavitation bubble or cloud collapses close enough to the solid wall, it will induce a high-speed micro-jet and shock waves, which can result in erosion [1]. Understanding the correct cavitation physics is important because then the adverse consequences such as erosion can be reduced.

Among the studies on cavitation, high-speed visualization is the most popular technique to investigate the cavitation. However, quantitative information regarding the vapor fraction is difficult to obtain from the high-speed imaging, because the cavitation bubbles scatter light and make the flow opaque. Recently, X-ray densitometry has been demonstrated as a valuable technique to quantify the void fractions in various cavitation related studies [2, 3, 4]. Void fractions are of high importance in the understanding of shedding behavior in the periodic cavitation. Recently Ganesh et al. [5] found that under particular conditions a condensation shock can be the dominant mechanism for periodic cavitation shedding, instead of the re-entrant jet. Time-resolved X-ray densitometry was used to investigate the local void fractions in the flow field. They found that void fractions increase with an increase in cavitation intensity. These experiments were performed on a 2D wedge. Although cavitation can also be observed in other test geometries, a converging-diverging nozzle (venturi) is used in this study. Due to its high contraction ratio, wider cavitation dynamic range can be achieved.

X-ray computed tomography is extensively used in medical imaging. It uses the relation between the material properties and the attenuation coefficient of X-rays. Images are created of the attenuation along the beam paths. This capability will be utilized in this study to examine the vapor fractions, and radial geometric characteristics in the flow.

2. Experimental details

2.1. Flow facility

A schematic overview of the experimental setup is given in Figure 1(a). The flow in the closed loop system is driven by a centrifugal pump, and a flowmeter is used to measure the volumetric flow rate. The measurements from the upstream pressure transducer, downstream pressure transducer, and the temperature sensor are used to determine the cavitation number σ. A water column is present at an angle due to space restrictions to collect the air bubbles entrained in the flow during degasification, and to vary the global static pressure of the system. A vacuum pump is used to control the global static pressure below ambient pressure.

*Corresponding Author, Saad Jahangir: S.Jahangir@tudelft.nl

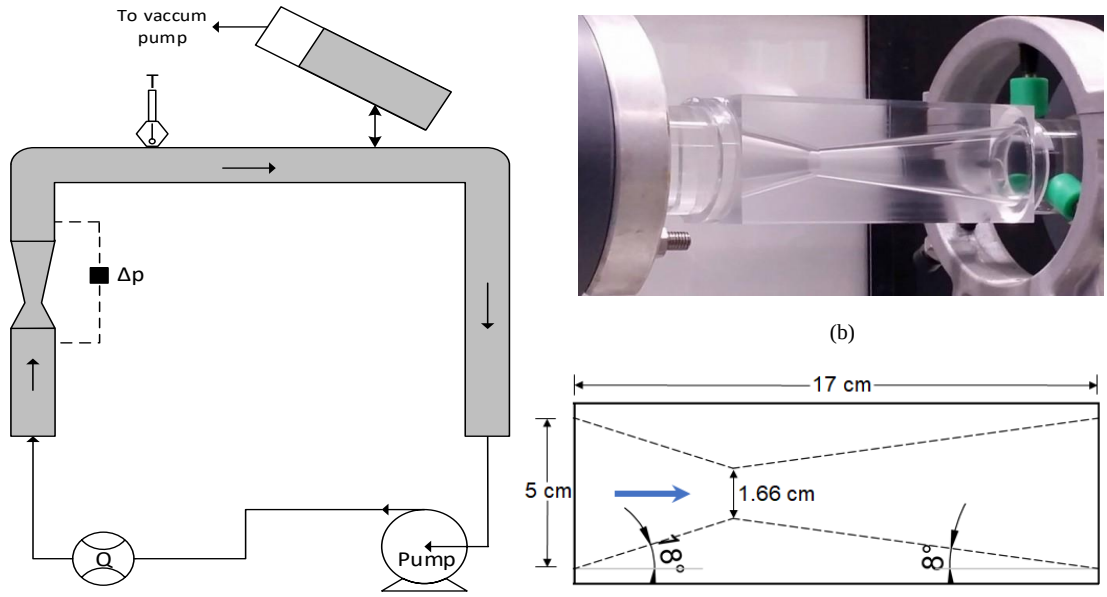

Figure. 1: (a) Schematic overview of the experimental setup. (b) Picture of the converging-diverging part (venturi) in the experimental setup. (c) The geometry and relevant dimensions of the venturi.

In Figure 1(b) and (c), a picture of the venturi can be seen with its geometrical parameters. The flow direction is from left to right in the figure, upward in reality. The convergence and divergence angles are 36° and 16°, respectively (inspired by previous studies: [6, 7, 8]). An area ratio of 1:9 (area of the throat versus exit area) is chosen. An oxygen sensor is used to determine the gas content in the system.

2.2. X-ray imaging

Figure 2(a) and (b) show a photograph of the measurement section in the X-ray setup and schematic overview of the method, respectively. A source-detector pair is used to measure the attenuation of the X-rays through the cavitating venturi. The source is operated at 120 keV and 5 mA in order to achieve a high contrast between the liquid and vapor phases within the venturi. The flat detector, Xineos-3131 CMOS model, consists of a 307×302 mm sensitive area. For the experiments, the field of view of 1548×660 pixels is chosen. Each pixel has a size of 198×198 μm with 14 bits of pixel depth. The images are recorded at 60 Hz during 1 min. As the typical shedding frequency is 40 Hz at σ = 0.46, this ensures that the statistics are based on sufficient shedding cycles.

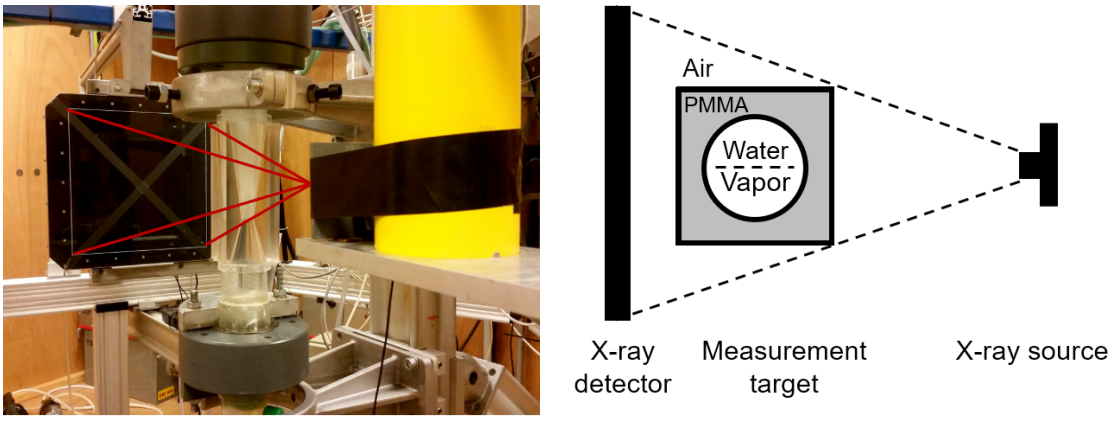

Figure. 2: (a) Test-rig inside the X-ray setup. (b) Sketch of the X-rays imaging method, the viewing angle in the experiments is smaller than the depicted angle.

2.3. Experimental procedure and post-processing

The water is degasified and the setup is operated for a few minutes before the measurements are started in order to obtain a uniform water temperature. The global static pressure of the system is set to a fixed value and the measurements are started when the pressure measurements are constant. All the sensor values (pressure, flow rate, and temperature) and the X-ray images (explained in more detail in the later paragraph) are saved concurrently by using a data acquisition system.

A background subtraction operation is performed for the raw X-ray images, for which background images with only the liquid phase without flow are captured. In order to improve the contrast, an image adjustment operation is performed on images. This process involves rescaling the grayscale intensities in order to have 1% of the data being saturated at low and high intensities. 3600 instantaneous X-ray images are averaged to get a representative time-averaged image, averaging also reduces the noise considerably. Calibration for the void fraction is done by inserting 5 empty thin-walled plastic cylinders of known, different diameters into the venturi filled with water, and X-ray images are obtained. The wall thickness of the plastic cylinders is very small, so it is neglected. The obtained calibration curve is used to calculate the void fractions for the reconstructed images (explained in the results).

Filtered back projection is applied to the cone-beam 2D time-averaged X-ray image (Figure 3) using the ASTRA Toolbox [9]. It is a stabilized and discretized version of the inverse Radon transform. Density slices of the object perpendicular to the centerline axis are created. As the measurement section is axisymmetric, we assume axisymmetry in the flow. The 3D reconstruction is performed with a time-averaged image obtained from the projections recorded at a single viewing angle.

3. Results

Figure 3(a) shows the time-averaged X-ray intensity data. This panel is before tomographic reconstruction, i.e. a projection along the line between source and detector. Figure 3(b) shows reconstructed slices at different axial positions, showing growth of the cavitation cloud. Figure 3(a) and (b) show that most of the vapor is attached to the nozzle wall and persists until 4 diameters downstream of the throat. This is the point where the cavity detaches during the periodic shedding, this is also confirmed from the high-speed images [10]. After detaching, the vapor cloud moves towards the center of the venturi and diffuses with the liquid phase.

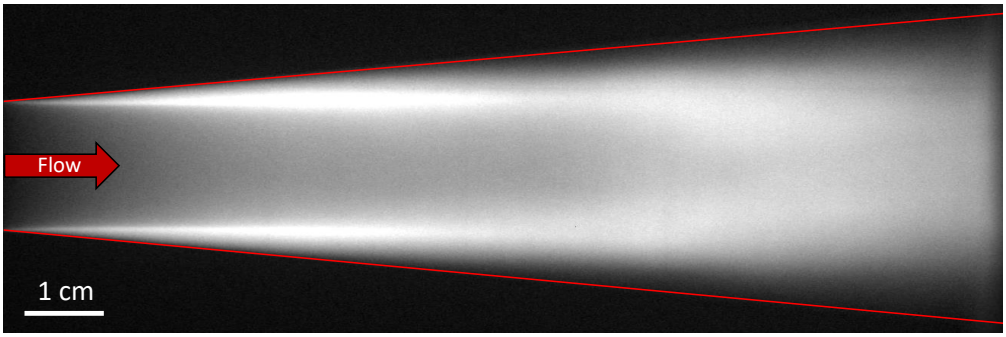

(a)

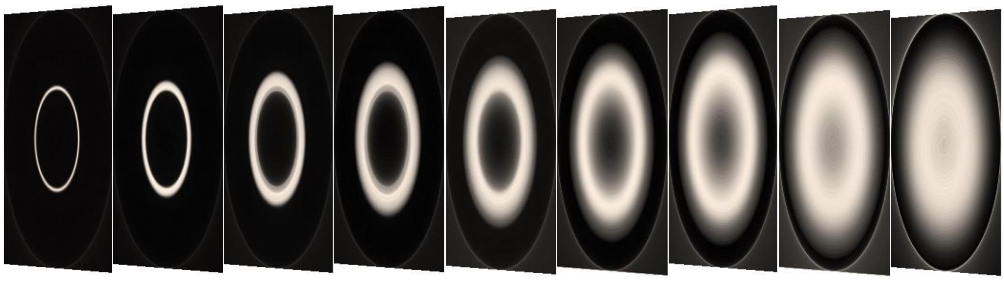

(b)

Figure. 3: (a) Time-averaged X-ray image of the cavitating venturi at $\sigma = 0.46$ (vapor is light gray, liquid is black). (b) Cross-sectional CT images at different axial positions showing growth of the cavitation cloud. The contrast in the images is adjusted for better understanding.

Figure 4 represents two slices from two different positions along the venturi length, where the vapor and liquid regions are shown in red and blue color, respectively. According to the calibration process discussed above and

the corresponding color bar, the vapor fraction can be obtained easily for every pixel of the slice. It can be seen from Figure 4(a) and (b), the cavitation changes from sheet cavitation to cloud cavitation with the interface diffusing downstream of the venturi. The void fraction decreases as the cavitation structures expand in the liquid core.

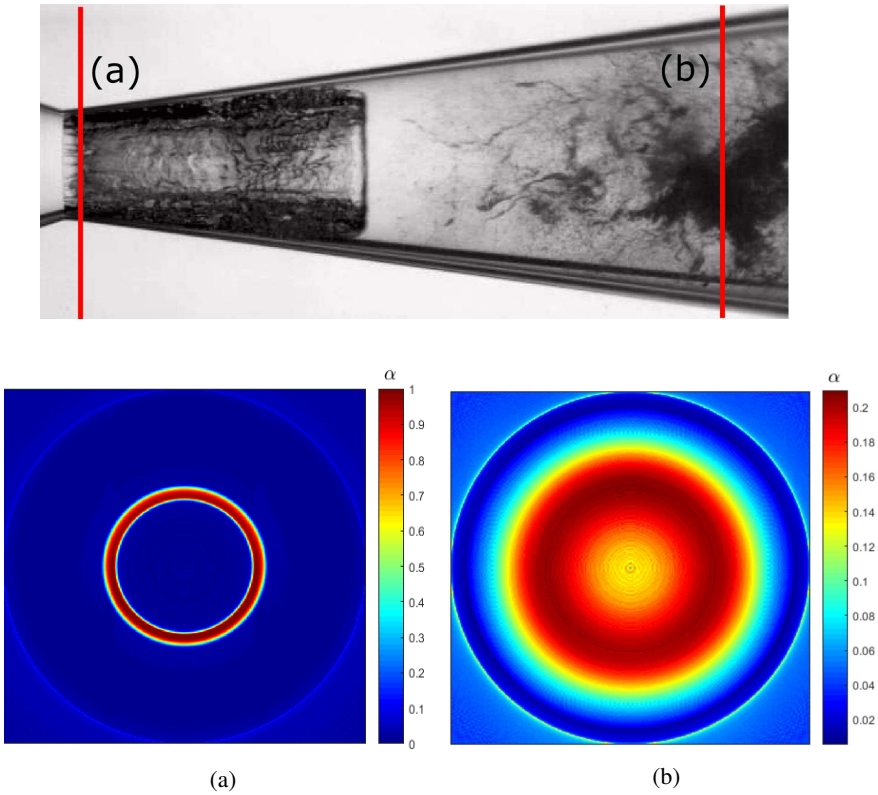

Figure. 4: (Top) A high-speed snapshot showing cavitation in the venturi. In (a) and (b), the quantitative measurements of vapor fractions at two different locations along the venturi are shown. The red regions indicate the presence of vapor and the blue regions indicate the presence of liquid. Note the difference in color scales.

4. Conclusions and Outlook

In this study, the phenomenon of cavitation was examined by CT measurements of the flow through a venturi. The results look encouraging in terms of time-averaged vapor fractions. More detailed information about the cavitation development is extracted using the cross-sectional CT-measurements as compared to the high-speed imaging. We can now quantify the radial geometric features of this complex two-phase flow. This data will be essential to validate our assumptions regarding the physical mechanisms. Furthermore, it will be helpful for the validation of numerical studies.

Acknowledgments

SJ has received funding from the European Union Horizon 2020 Research and Innovation programme, Grant Agreement No 642536. CP has received funding from ERC Consolidator Grant "OpaqueFlows".

References

[1] C. Peng, S. Tian, and G. Li, "Joint experiments of cavitation jet: High-speed visualization and erosion test," *Ocean Engineering*, vol. 149, pp. 1–13, 2018.

[2] I. Khlifa, A. Vabre, M. Hočevar, K. Fezzaa, S. Fuzier, O. Roussette, and O. Coutier-Delgosha, "Fast x-ray imaging of cavitating flows," *Experiments in Fluids*, vol. 58, no. 11, p. 157, 2017.

[3] N. Mitroglou, M. Lorenzi, M. Santini, M. Gavaises, and D. Assanis, "Application of cone-beam micro-CT on high-speed Diesel flows and quantitative cavitation measurements," in *Journal of Physics: Conference Series*, vol. 656, p. 012094, 2015.

[4] D. Bauer, H. Chaves, and C. Arcoumanis, "Measurements of void fraction distribution in cavitating pipe flow using x-ray CT," *Measurement Science and Technology*, vol. 23, no. 5, p. 055302, 2012.

[5] H. Ganesh, S. A. Mäkiharju, and S. L. Ceccio, "Bubbly shock propagation as a mechanism for sheet-to-cloud transition of partial cavities," *Journal of Fluid Mechanics*, vol. 802, pp. 37–78, 2016.

[6] X. Long, J. Zhang, J. Wang, M. Xu, Q. Lyu, and B. Ji, "Experimental investigation of the global cavitation dynamic behavior in a venturi tube with special emphasis on the cavity length variation," *International Journal of Multiphase Flow*, vol. 89, pp. 290–298, 2017.

[7] S. Hayashi and K. Sato, "Unsteady Behavior of Cavitating Waterjet in an Axisymmetric Convergent-Divergent Nozzle: High Speed Observation and Image Analysis Based on Frame Difference Method," *Journal of Flow Control, Measurement & Visualization*, vol. 2, pp. 94–104, 2014.

[8] P. Tomov, S. Khelladi, F. Ravelet, C. Sarraf, F. Bakir, and P. Vertenoeuil, "Experimental study of aerated cavitation in a horizontal venturi nozzle," *Experimental Thermal and Fluid Science*, vol. 70, pp. 85–95, 2016.

[9] W. van Aarle, W. J. Palenstijn, J. Cant, E. Janssens, F. Bleichrodt, A. Dabravolski, J. De Beenhouwer, K. J. Batenburg, and J. Sijbers, "Fast and flexible X-ray tomography using the ASTRA toolbox," *Optics express*, vol. 24, no. 22, pp. 25129–25147, 2016.

[10] W. J. Hogendoorn, "Cavitation: Experimental investigation of cavitation regimes in a coverging-diverging nozzle," *Master's thesis, Delft University of Technology*, 2017. Available online at uuid:823a18f0-66a8-4ffd-a688-c3dadf62c4da.